Vegetation Interaction Enhances Interdecadal Climate Variability in the Sahel

Ning Zeng[1], J. David Neelin, William K.-M. Lau

July 13, 1999

[1]N. Zeng and J. D. Neelin are at the Department of Atmospheric Sciences and Institute of Geophysics and Planetary Physics, University of California, Los Angeles, CA 90095-1565. Email: zeng@atmos.ucla.edu; W. K.-M. Lau is at the Climate and Radiation Branch, NASA-Goddard Space Flight Center, Greenbelt, Maryland. [1]To whom correspondence should be addressed.

Abstract

The role of naturally varying vegetation in influencing the climate variability in the Sahel is explored in a coupled atmosphere-land-vegetation model. The Sahel rainfall variability is influenced by sea surface temperature (SST) variations in the oceans. Land-surface feedback is found to increase this variability both on interannual and interdecadal time scales. Interactive vegetation enhances the interdecadal variation significantly, but can reduce year to year variability due to a phase lag introduced by the relatively slow vegetation adjustment time. Variations in vegetation accompany the changes in rainfall, in particular, the multi-decadal drying trend from the 1950s to the 80s.

Figure 1A shows the observed rainfall over the West African Sahel region (1) from 1950 to 1998. It shows a multi-decadal drying trend from the 1950s to the 80s and early 90s, as well as strong interannual variability. Proposed mechanisms for this dramatic trend include global sea surface temperature variations (2–5) and land-use change, i.e., the desertification process (6–7). Since vegetation distribution tends to be largely controlled by climate (8–9), and surface property change can impact the climate by modifying the atmospheric energy and water budget (10–12), it is reasonable to conjecture that dynamic vegetation-climate interaction might influence the climate variability substantially in a climatically sensitive zone like the Sahel. We test this hypothesis in a coupled atmosphere-land-vegetation model of intermediate complexity.

The atmospheric component of the coupled model used here is the Quasi-equilibrium Tropical Circulation Model (QTCM) (13, 14), which is coupled to the land-surface model Simple-Land (SLand) (14) which represents the first-order effects relevant to climate simulation. The QTCM simulates a seasonal climate over the Sahel that is close to observations and that compares favorably with current atmospheric general circulation models (GCMs). We model the major effects on climate of a varying vegetation through its control of the evapotranspiration process and modification

of the surface albedo. Other effects, such as surface roughness and modification of soil properties, are not considered here.

Vegetation growth in the tropics is less influenced by temperature and nutrient limitation, but is mainly controlled by water availability on the interannual and decadal time scales because of the relatively large rainfall variability. The central equation in the dynamic vegetation model is a biomass equation driven by photosynthesis and vegetation loss:

$$\frac{dV}{dt} = a\beta(w)(1 - e^{-kL}) - V/\tau \tag{1}$$

where a is a carbon assimilation coefficient, β is the soil moisture dependence as used in the original SLand, L is the plant leaf area index (LAI), and k is the extinction coefficient of photosynthetically active sunlight. The vegetation time scale τ is taken as one year in the following experiments. This is similar to the biomass equations used in models with more explicit vegetation dynamics (15–18). V is interpreted as vegetation amount or leaf biomass and it is normalized between 0 and 1. The LAI is assumed directly proportional to V as $L = L_{max}V$, where L_{max} is a maximum LAI taken as 8. The current version does not explicitly model plant competition, nor does it consider species-specific characteristics such as resources allocation. The seasonality is not explicitly modeled for V, so Eq. 1 represents variation on the background of a mean seasonal cycle.

The original version of the land model is modified to account for the effects of leaf-to-canopy scaling (19) such that the canopy conductance for evapotranspiration is:

$$g_c = g_{s_{max}}\beta(w)(1 - e^{-kL})/k \tag{2}$$

where $g_{s_{max}}$ is a leaf-level maximum conductance. Note that photosynthesis and evapotranspiration are closely related in Eq. 1 and Eq. 2 (19). Besides modifying evapotranspiration through Eq. 2, vegetation also changes land-surface albedo A as (20)

$$A = 0.38 - 0.3(1 - e^{-kL}). \tag{3}$$

This corresponds to an albedo of 0.38 at $V = 0$ (desert), and 0.09 at maximum vegetation $V = 1$ (dense forest). Thus, vegetation feeds back into the atmosphere by modifying evapotranspiration and surface albedo through Eq. 2 and Eq. 3.

In order to identify the relative importance of oceanic forcing, land-surface and vegetation processes, we perform a series of model experiments, starting from a run in which both land and vegetation are interactive (the default and realistic case), designated as LonVon. The monthly output from this run is then used to derive a vegetation climatology (with a seasonal cycle but which does not change from year to year) which is used as a model boundary condition for the second run LonVoff. The output of the run LonVoff is then used to derive a soil moisture climatology which is used to drive the third experiment LoffVoff. In all these three runs, the coupled atmosphere-land-vegetation model is driven by the observed monthly SST from 1950 to 1998 (21). All three start from an initial condition taken from an interactive land/vegetation run forced by a climatological SST. The model simulated annual rainfall over the Sahel from these experiments is shown in Fig. 1B-D.

Compared to the observations in Fig. 1A, the LoffVoff run with non-interactive soil moisture and vegetation (Fig. 1B) shows a weak interannual variation, and a much weaker interdecadal signal, although a drying trend can be seen from the 1950s to the 80s. The interactive soil moisture (Fig. 1C) appears to somewhat increase this interdecadal drying trend all the way into the early 90s. The simulated soil moisture shows a high degree of correlation with precipitation. The amplitude of interannual variation is also larger in general, in agreement with other studies (22–24).

By allowing vegetation feedback to the atmosphere, the decadal rainfall variability is enhanced significantly (Fig. 1D). The wet periods in the 1950s and the dry periods in the 70s and the 80s stand out and are much more like in the observations. Compared to the non-interactive vegetation case LonVoff, the interannual variability does not show apparent enhancement. In some cases, the year to year change such as from the dry 1987 to the relatively wet 1988 is actually reduced, because the vegetation is still low from the previous drought due to its relatively slow response. This complicated lagged relationship between vegetation and precipitation is also seen in observations (25), but our

understanding of vegetation dynamics and the modeling tools available are at present not sufficient for a precise assessment. The variation in the rainfall drives a similar trend in vegetation through vegetation growth or loss (Fig. 1D). The vegetation lags slightly behind the rainfall and its variation is also smoother, although these tendencies are not very strong because the one year vegetation time scale used in the model runs is comparable to the time resolution of the plot.

In order to assess the internal climate variability in the model, three 9-member ensemble runs have been conducted corresponding to the cases above. The member runs in an ensemble differ only in their initial atmospheric and soil moisture conditions. We use the Sahel rainfall difference between the wet period 1950–67 and the dry period 1968–87 as an indicator of the amplitude of the interdecadal variation. Figure 2 shows the successive amplification of the decadal trend with the inclusion of interactive soil moisture and especially, vegetation. However, even the LonVon case still tends to underestimate the observed decadal trend. Furthermore, the scatter among the ensemble members also increases when additional feedbacks are included. Interactive vegetation increases the variance even though vegetation initial conditions are identical in these runs.

The interactive vegetation modifies the precipitation through a chain of positive feedback loops. For instance, decreased rainfall leads to less water availability and reduces vegetation, which in turn leads to higher surface albedo and reduced evapotranspiration. This weakens the large-scale atmospheric circulation by reducing the energy and water flux into the atmosphere column, thus further decreasing the local rainfall (6, 10, 12, 26).

The dynamic nature of the vegetation-climate interaction can be understood more precisely in a linear system by simplifying these feedback processes:

$$\frac{dV'}{dt} = \frac{\alpha P' - V'}{\tau} \tag{4}$$

$$P' = \mu V' + F_0 e^{i\omega t} \tag{5}$$

Here V' and P' are perturbations to vegetation and precipitation respectively, and they approximate the interannual/interdecadal anomalies shown above. The coefficients α and μ represent the

strength of the local interaction between vegetation and the atmosphere. Equation 4 is a linearized version of the biomass equation (Eq. 1) because soil moisture is forced by precipitation, and Eq. 5 approximates the vegetation feedback to rainfall through changes in surface albedo in Eq. 3 and evapotranspiration in Eq. 2. The rainfall is sinusoidally forced at frequency ω and amplitude F_0, representing the SST-induced change in the large-scale atmospheric circulation.

The dependences on ω of the amplitude of P' and phase lag ϕ are shown in Fig. 3 (27). At low frequency forcing ($\omega\tau \rightarrow 0$), vegetation has enough time to establish a near equilibrium with the precipitation, consequently the precipitation is enhanced by a factor of $1/(1-\alpha\mu)$ with little phase lag. This explains the amplification of the interdecadal variation of rainfall shown in Fig. 1D. At high frequency forcing ($\omega\tau \rightarrow \infty$), vegetation has little time to respond to the forcing due to its relatively long adjustment time, therefore, the precipitation variation is mostly a direct response to the forcing. At intermediate frequency forcing, the amplitude is enhanced slightly, but the phase lag is at a maximum. This phase lag has significant consequences for the interannual variability. In 1988, for instance, the memory in vegetation of the previous drought years has delayed and reduced the otherwise strong wetting tendency resulting from SST-induced atmospheric circulation change (cf. Fig. 1C and D).

The model simulated Sahel rainfall in LonVon shows a correlation with the observation of 0.67, a significant improvement from a 0.44 correlation in LonVoff. However, the year to year comparison with the observations is not as satisfactory. When we decompose the Sahel rainfall time series into low frequency (longer than 10 years) and high frequency (shorter than 10 years) components, the correlation with the observation is only 0.1 at high frequency and 0.94 at low frequency for the LonVon run. The discrepancy in the interannual simulation, both in our model and in the GCMs (4, 28), is not necessarily due to model deficiencies, since considerable variability arises from the chaotic nature of the atmosphere-land-vegetation system.

While we focus on natural climate variations involving vegetation changes, this does not exclude any role anthropogenic land-use change might play. Indeed it is possible that the anthropogenic

factor might account for the remaining difference between the interactive vegetation run and observations in Fig. 2 on decadal time scales. But because the vegetation feedback acts to amplify Sahel rainfall variability that originates from SST variations, significant effects can occur with relatively small vegetation changes. In the experiment with interactive vegetation (Fig. 3D), the change of surface albedo (not shown) on the interdecadal time scale is about 0.03. This is a subtle change compared either to the albedo change values of 0.1 used in GCM desertification experiments (6), or to what could be estimated from satellite observations in earlier decades. Current satellite systems will be capable of measuring this level of variation for future decadal fluctuations. The present results suggest the importance of such measurements, due to the role vegetation feedbacks can play in interannual/interdecadal climate variability in climatically sensitive zones like the Sahel.

References and Notes

1. Rainfall, based on the surface gauge data from M. Hulme ["Validation of large-scale precipitation fields in *Global precipitations and climate change*, M. Desbois and F. Desalmand, Eds. (NATO ASI Series, Springer-Verlag, Berlin, 1994) pp. 466] averaged over 15W-20E, 13N-20N, which approximately corresponds to the Sahel region as defined by S. E. Nicholson ["Variability of African rainfall on interannual and decadal time scale" in *Natural Climate Variability on Decade-to-Century Time Scales*, (National Research Council, National Academy Press, Washington, DC, 1995) pp. 630].

2. C. K. Folland, T. N. Palmer, and D. E. Parker, *Nature*, **320**, 602 (1986).

3. D. P. Rowell, C. K. Folland, K. Maskell, and M. N. Ward, *Quart. J. Roy. Meteor. Soc.*, **121, Part A**, 669 (1995).

4. D. P. Rowell, *Quart. J. Roy. Meteor. Soc.*, **122**, 1007, (1996).

5. F. H. M. Semazzi, B. Burns, N.-H. Lin, and J.-K. Schemm, *J. Climate*, **9**, 2480 (1996).

6. Y. Xue and J. Shukla, *J. Climate*, **5**, 2232 (1993).

7. P. A. Dirmeyer and J. Shukla, *Quart. J. Roy. Meteor. Soc.*, **122**, 451 (1996).

8. L. R. Holdridge, *Science*, **105**, 367 (1947).

9. F. I. Woodward, *Climate and Plant Distribution*, (Cambridge University Press, 1987), pp.174.

10. J. G. Charney, *Quart. J. Roy. Meteor. Soc.*, **101**, 193 (1975).

11. J. Shukla and Y. Mintz, *Science*, **215**, 1498 (1982).

12. R. E. Dickinson, in *Climate System Modeling*, K. E. Trenberth, Ed. (Cambridge University Press, 1992), pp. 689–701.

13. J. D. Neelin and N. Zeng, *J. Atmos. Sci.*, in press.

14. N. Zeng, J. D. Neelin, and C. Chou, *J. Atmos. Sci.*, accepted.

15. H. H. Shugart, *A theory of forest dynamics: the ecological implications of forest succession models*, (Springer-Verlag, New York, 1984), pp. 278.

16. J.-J. Ji, *J. Biogeogr.*, **22**, 445 (1995).

17. J. A. Foley et al., *Global Biogeochem. Cycles*, **10**, 603 (1996).

18. R. E. Dickinson, M. Shaikh, R. Bryant, and L. Graumlich, *J. Climate*, **11**, 2823 (1998).

19. P. J. Sellers et al., *J. Climate*, **9**, 676 (1996).

20. Verstraete, M., B. Pinty, and R. E. Dickinson, *J. Geophys. Res.*, **95**, 755 (1990).

21. R. W. Reynolds and T. M. Smith, *J. Climate*, **7**, 929 (1994).

22. T. L. Delworth and S. Manabe, *Advances in Water Resources*, **16**, 3 (1993).

23. R. D. Koster and J. J. Suarez, *J. Geophys. Res.*, **100**, 13775 (1995).

24. K.-M. Lau and W. Bua, *Climate Dynamics*, **14**, 759 (1998).

25. S. N. Goward and S. D. Prince, *J. Biogeogr.*, **22**, 549 (1995).

26. N. Zeng and J. D. Neelin, *J. Climate*, **12**, 857 (1999).

27. The solutions of Eqs. 4–5 for the oscillation amplitude and phase shift ϕ relative to the forcing for P' are

$$|\frac{P'}{F_0}|^2 = \frac{1+\omega^2\tau^2}{(1-\alpha\mu)^2}$$

$$\tan(\phi) = -\frac{\alpha\mu\omega\tau}{1-\alpha\mu+\omega^2\tau^2}$$

For conditions on the approximations in Eq. 5, see Zeng and Neelin (1999) (14). The coupling coefficients α and μ are positive and $\alpha\mu < 1$ so that the positive feedbacks do not become unstable. In Fig. 3, $\alpha\mu = 0.5$.

28. K. R. Sperber and T. N. Palmer, *J. Climate*, **9**, 2727 (1996).

29. C. J. Tucker, H. E. Dregne, and W. W. Newcomb, *Science*, **253**, 299 (1991).

30. Supported by NSF grant ATM-9521389, NOAA grant NA86GP0314 and a grant to N. Zeng from the NASA IPA program.

List of Figures

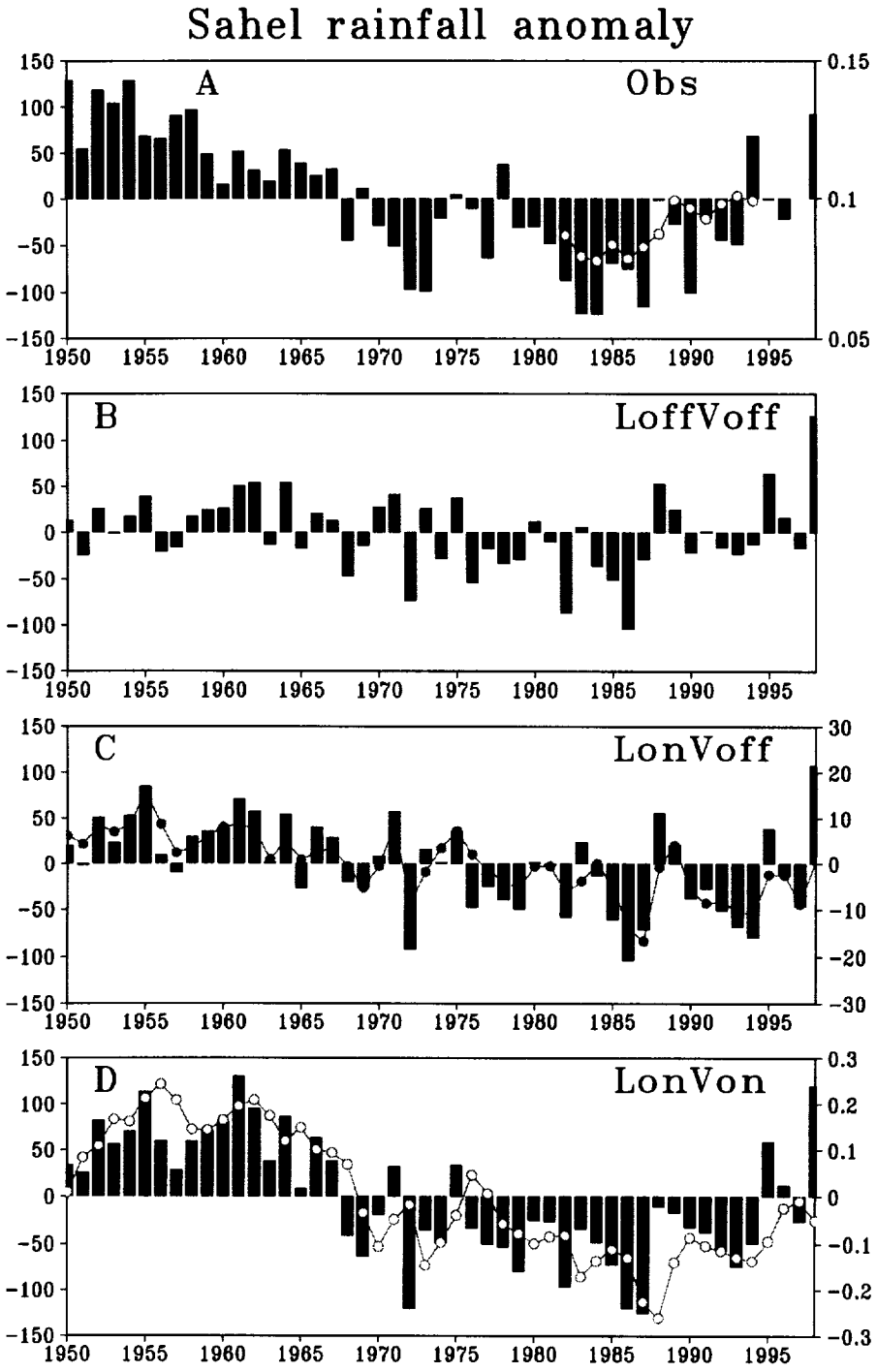

Figure 1: Annual rainfall anomaly in mm y^{-1} (vertical bars) over the West African Sahel (13N–20N, 15W–20E) from from 1950 to 1998: (A) observations from Hulme (1) (B) model with non-interactive land-surface hydrology (fixed soil moisture) and non-interactive vegetation (SST influence only, LoffVoff); (C) model with interactive soil moisture but non-interactive vegetation (LonVoff); (D) model with interactive soil moisture and vegetation (LonVon); showing the role of interactive soil moisture and vegetation in enhancing the SST-induced interdecadal rainfall variability from the 1950s to the 1990s, and also modifying the interannual variability. Also plotted (as connected circles; labeled on the right) are: (A) the Normalized Difference Vegetation Index (NDVI) (28); (C) model simulated annual soil moisture anomaly (mm); (D) model simulated leaf area index (LAI) anomaly. All the anomalies are computed relative to the 1950–98 base period.

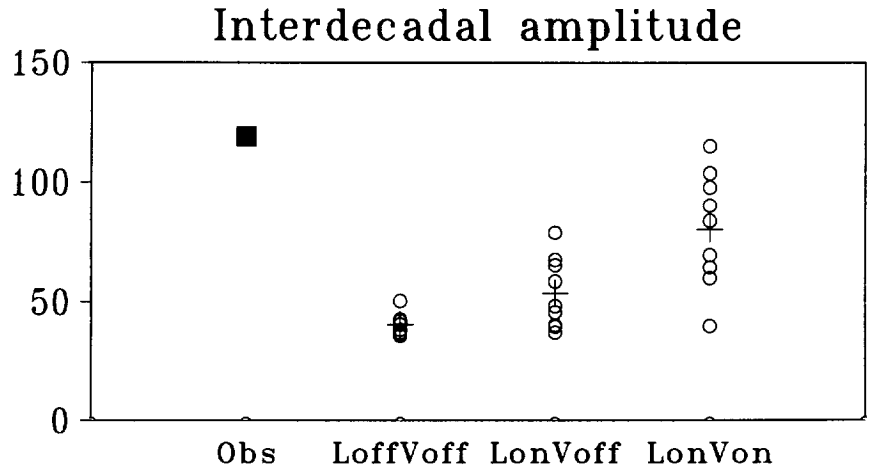

Figure 2: Sahel rainfall difference between the period 1950–67 and the period 1968–87 for observations (filled square) and three 9-memeber ensemble runs with and without interactive soil moisture and vegetation, similar to the ones in Fig. 1B-D. Open circles denote individual ensemble members with different initial conditions and hence different chaotic internal variability. Crosshairs denote ensemble means. In mm y^{-1}.

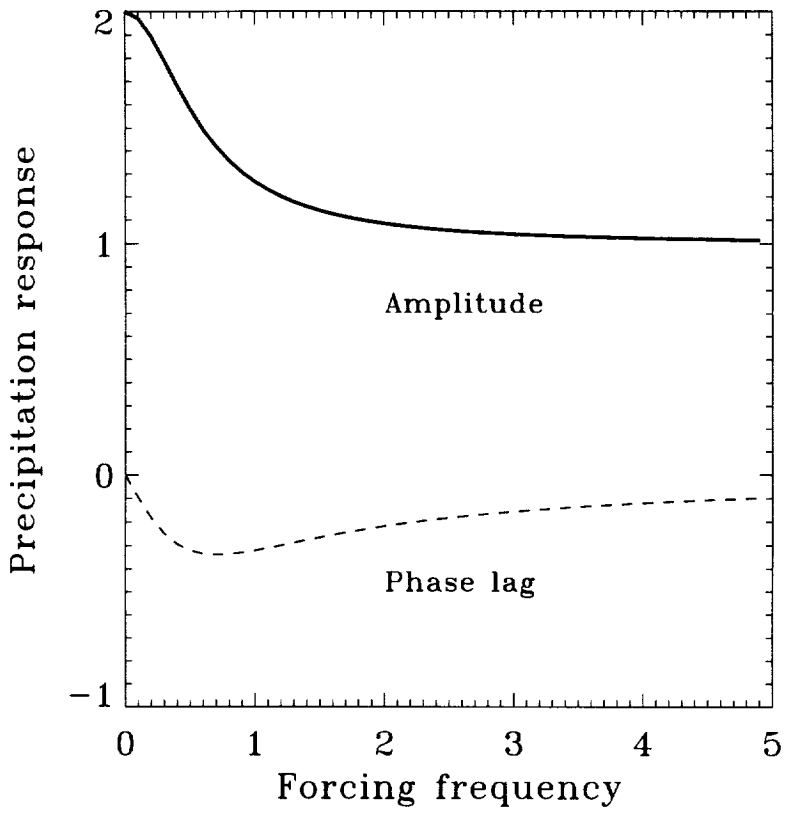

Figure 3: Response of rainfall to a sinusoidal forcing in the idealized linear system (Eqs. 4, 5), illustrating the dependence of vegetatioin feedback on forcing frequency. The response amplitude (P'/F_0, solid line) and phase lag (ϕ, in radians, dashed line) are plotted as a function of the forcing frequency $\omega\tau$ (normalized by the vegetation time scale τ).